ADVANCED MATERIALS
www.advmat.de

Corannulene-Incorporated AIE Nanodots with Highly Suppressed Nonradiative Decay for Boosted Cancer Phototheranostics In Vivo

Xinggui Gu, Xiaoyan Zhang, Huili Ma, Shaorui Jia, Pengfei Zhang, Yanjun Zhao, Qian Liu, Jianguo Wang, Xiaoyan Zheng, Jacky W. Y. Lam, Dan Ding, and Ben Zhong Tang**

Fluorescent nanoparticles (NPs) based on luminogens with aggregation-induced emission characteristic (AIEgens), namely AIE dots, have received wide attention because of their antiquenching attitude in emission and reactive oxygen species (ROS) generation when aggregated. However, few reports are available on how to control and optimize their fluorescence and ROS generation ability. Herein, it is reported that enhancing the intraparticle confined microenvironment is an effective approach to advanced AIE dots, permitting boosted cancer phototheranostics in vivo. Formulation of a "rotor-rich" and inherently charged near-infrared (NIR) AIEgen with 1,2-distearoyl-sn-glycero-3-phosphoethanolamine-N-[methoxy(polyethylene glycol)-2000] and corannulene-decorated PEG affords DSPE-AIE dots and Cor-AIE dots, respectively. Compared to DSPE-AIE dots, Cor-AIE dots show 4.0-fold amplified fluorescence quantum yield and 5.4-fold enhanced ROS production, because corannulene provides intraparticle rigidity and strong interactions with the AIEgen to restrict the intramolecular rotation of AIEgen to strongly suppress the nonradiative decay and significantly facilitate the fluorescence pathway and intersystem crossing. Thus, it tremendously promotes phototheranostic efficacies in terms of NIR image-guided cancer surgery and photodynamic therapy using a peritoneal carcinomatosis-bearing mouse model. Collectively, it not only provides a novel strategy to advanced AIE dots for cancer phototheranostics, but also brings new insights into the design of superior fluorescent NPs for biomedical applications.

Development of optical agents for cancer phototheranostics has recently attracted great interest as they allow for real-time molecular diagnosis and concurrent light-triggered treatment.[1–8] Among various phototheranostic agents, fluorescent nanoparticles (NPs) are receiving broader attention due to their combined merits in terms of high sensitivity and temporal resolution of fluorescence imaging technique, on-demand and in situ signature of photodynamic therapy (PDT) as well as unique enhanced permeability and retention (EPR) effect of nanomaterials.[9–14] To meet the requirements of ideal cancer phototheranostics, the fluorescent NPs must have several necessary qualities: 1) sufficiently high near-infrared (NIR) emission (>650 nm) and reactive oxygen species (ROS) generation efficiency of fluorescent component within NPs; 2) strong resistance to photobleaching; 3) negligible cytotoxicity and in vivo toxicity; and 4) suitable NP size and surface chemistry,[15] permitting prominent EPR effect. Compared with other extensively investigated fluorescent NPs, organic fluorophore-doped NPs hold the advantages of tunable photophysical properties, flexible structural tailoring, and good biocompatibility.[16] However, these π-conjugated fluorophores tend to

Prof. X. Gu, Dr. J. Wang, P. Zhang, Dr. X. Zheng, Dr. J. W. Y. Lam, Prof. B. Z. Tang
Department of Chemistry
Hong Kong Branch of Chinese National Engineering Research Center for Tissue Restoration and Reconstruction
Division of Life Science
State Key Laboratory of Molecular Neuroscience
Institute for Advanced Study
and Division of Biomedical Engineering
The Hong Kong University of Science and Technology
Clear Water Bay, Kowloon, Hong Kong, China
E-mail: tangbenz@ust.hk

Prof. X. Gu
Beijing Advanced Innovation Center for Soft Matter Science and Engineering
Beijing University of Chemical Technology
Beijing 100029, China

The ORCID identification number(s) for the author(s) of this article can be found under https://doi.org/10.1002/adma.201800403.

DOI: 10.1002/adma.201801065

X. Zhang, S. Jia, Prof. D. Ding
State Key Laboratory of Medicinal Chemical Biology
Key Laboratory of Bioactive Materials
Ministry of Education
and College of Life Sciences
Nankai University
Tianjin 300071, China
E-mail: dingd@nankai.edu.cn

Dr. H. Ma
Key Laboratory of Flexible Electronics (KLOFE) & Institute of Advanced Materials (IAM)
Nanjing Tech University (Nan-jingTech)
30 South Puzhu Road, Nanjing 211800, China

Dr. Y. Zhao
School of Pharmaceutical Science & Technology
Tianjin Key Laboratory for Modern Drug Delivery & High Efficiency
and Collaborative Innovation Center of Chemical Science and Engineering (Tianjin)
Tianjin University
Tianjin 300072, China

aggregate within NPs. For conventional small-molecule fluorescent dyes with planner molecular structures, such aggregation within NPs often causes significant quenching of light emission and ROS production owing to intermolecular interactions such as π–π stacking and other nonradiative decays, which tremendously limit their application in cancer phototheranostics.[17,18] Much effort has been devoted to overcome the aggregation-caused quenching (ACQ) effect within fluorescent NPs through the introduction of bulky side groups and hydrophobic counterions into fluorophores.[17] For example, it has been recently reported that bulky tetrakis(pentafluorophenyl)borate counterion could enable the preparation of Cy5 dye-loaded NPs with high emission efficiency.[17b] However, the desired systems with excellent properties in both emission and ROS generation are still limited as a result of the difficulties to block the strong π–π stacking. Thereby, it is urgently desirable to develop direct and effective approaches to advanced fluorescent NPs with both high fluorescence and ROS generation capacity for cancer phototheranostics.

Aggregation-induced emission luminogens (AIEgens) have recently emerged as an alternative fluorescent material to construct fluorescent NPs, which perfectly address the challenge of ACQ and show low in vivo side toxicities.[19–24] AIEgens are often nonemissive in solution due to the consumption of the excited state energy via nonradiative relaxation by intramolecular motion. Upon aggregated, such relaxation from the lowest excited singlet state (S_1) to the ground state (S_0) is largely restricted due to the steric hindrance, leading to the energy of S_1 going through the fluorescence pathway to S_0.[21] This uncommon feature makes AIEgens ideal for fabrication of fluorescent NPs (usually named as AIE dots) with ultrahigh brightness and photobleaching threshold. Besides, our and several other groups have reported that for some AIEgens, the intersystem crossing (ISC) process from S_1 to the lowest excited triplet state (T_1) would facilely occur because of the designed small S_1-T_1 energy gap, followed by ROS production via energy transfer (ET) from T_1 to ambient oxygen (O_2), allowing for photodynamic cancer ablation.[19,20,25–29] Despite of these pioneer studies, there has been nearly no report on how to control and optimize the fluorescence and ROS generation ability of AIE dots by tuning the photophysical property. As superior fluorescent NPs with extremely high efficacy of cancer phototheranostics are always in high pursuit, we are motivated to develop a molecular guideline to simultaneously amplify the effectiveness of both fluorescence imaging and PDT of AIE dots.

In this contribution, we report for the first time that enhancing the intraparticle confined microenvironment is an effective new approach to advanced AIE dots, permitting boosted cancer phototheranostics in vivo. As a proof-of-concept, a new NIR emissive AIEgen (4-(2,2-bis(4-(diphenylamino)phenyl)-1-(4-methoxyphenyl)vinyl)-1-methylpyridinium hexafluorophosphate, namely TPP-TPA; **Figure 1**A) with "rotor-rich" skeleton and an inherent charge is designed and synthesized. Formulation of TPP-TPA using 1,2-distearoyl-sn-glycero-3-phosphoethanolamine-*N*-[methoxy(polyethylene glycol)-2000] (DSPE-PEG) and corannulene-decorated PEG (Cor-PEG) afforded two types of AIE dots, DSPE-AIE dots and Cor-AIE dots, respectively. Due to the large dipole moment of 2.1 D, superhydrophobicity, and hyper-rigidity of bowl-shape corannulene,[30–32] Cor-AIE dots is endowed with more intraparticle rigid microenvironments than DSPE-AIE dots. Compared to DSPE-AIE dots with relatively low NIR fluorescence and weak ROS generation capability, Cor-AIE dots show 4.0-fold amplified fluorescence quantum yield and 5.4-fold enhanced ROS production. The results including ^{1}H NMR titration and theoretical calculation essentially demonstrate that the corannulene providing intraparticle rigidity and strong interactions with TPP-TPA plays a key role in forceful restriction of intramolecular rotation of the encapsulated TPP-TPA, leading to highly suppressed nonradiative decay. The absorbed energy thus significantly flows to both the fluorescence pathway and ISC process. Such highly amplified NIR emission and ROS generation capacity are tremendously beneficial to the phototheranostic efficacies in terms of NIR image-guided cancer surgery and photodynamic cancer therapy using a peritoneal carcinomatosis-bearing mouse model. Since to date, DSPE-PEG is the most widely used encapsulation matrix for building AIE dots, this study with comparison results not only provides a new strategy and molecular guideline to prepare superior AIE dots, but also brings new insights into the design of advanced fluorescent NPs for biomedical applications.

The chemical structure of inherently charged TPP-TPA was shown in Figure 1A. To extend the emission spectrum to NIR range, two electron-donating diphenylamine groups and one electron-withdrawing 1-methylpyridinium unit were incorporated into the triphenylethene. Such strong electron donor–acceptor interactions endow TPP-TPA with a large dipole moment and the large number of rotatable aryl rings makes the skeleton of TPP-TPA flexible. The whole synthetic route of TPP-TPA was displayed in Figure 1A. Compound **1** was obtained with a high yield of 95% according to the procedure reported previously,[33] subsequently reacted with (4-methoxyphenyl)-pyridin-4-yl-methanone undergoing McMurry coupling to yield compound **2** in 70%. Finally, reaction of compound **2** with iodomethane followed by ion-exchange reaction with potassium hexafluorophosphate gave the desirable product TPP-TPA in a high yield of 99%. All intermediates and product were characterized by NMR and mass spectroscopies, from which satisfactory data corresponding to their structures were obtained (see Figures S1–S6, Supporting Information).

UV–vis absorption and photoluminescence (PL) spectra of TPP-TPA were recorded in Figure 1B; and Figure S7, Supporting Information. TPP-TPA absorbs at 440 nm with the absorption tail extended to 600 nm in dimethylsulfoxide (DMSO), covering most of visible light range. Such solution emits almost no light even increasing the water fraction (f_w) in DMSO-H_2O mixture up to 50%, ascribing to the active intramolecular rotation of the aryl rings (Figure 1C). Then the emission of TPP-TPA enhanced dramatically upon the f_w is over 50%. Together with the plot of

Dr. Q. Liu
Department of Urology
Tianjin First Central Hospital
Tianjin 300192, P. R. China
Prof. B. Z. Tang
NSFC Center for Luminescence from Molecular Aggregates
SCUT-HKUST Joint Research Institute
State Key Laboratory of Luminescent Materials and Devices
South China University of Technology
Guangzhou 510640, China

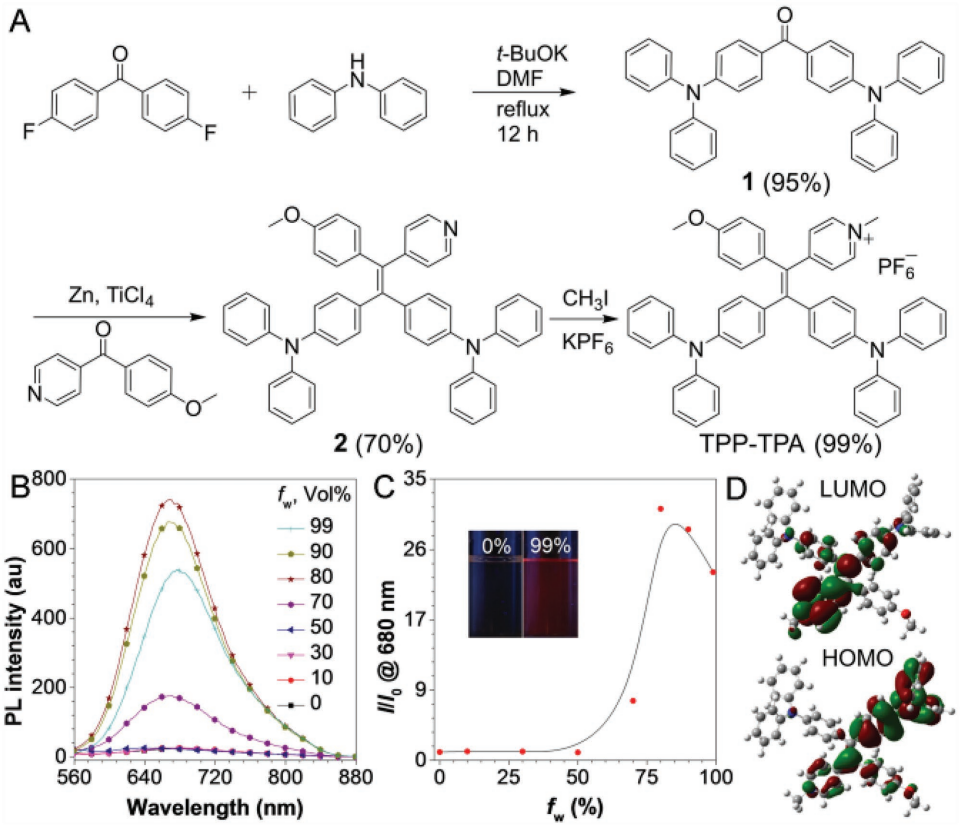

Figure 1. A) Synthetic route of NIR-emissive TPP-TPA. B) PL spectra of TPP-TPA in DMSO-H_2O mixtures with different water fractions (f_w). C) Plot of the relative PL intensity (I/I_0) at 680 nm versus f_w of the DMSO-H_2O mixture of TPP-TPA. Excitation wavelength: 440 nm. Insets show the fluorescent photos of TPP-TPA in DMSO and DMSO-H_2O mixture with the f_w of 99% taken under 365 nm UV lamp. Concentration of TPP-TPA: 10×10^{-6} M. D) Molecular orbital amplitude plots of HOMO and LUMO for TPP-TPA in ground states based on density functional theory (DFT) calculation under the method of opt wB97XD/6-31g**.

emission intensity at 680 nm against f_w and the inset fluorescent photos of the red emission in the 99% aggregated solution compared to the negligible emission in DMSO (Figure 1C), TPP-TPA exhibited the typical AIE characteristic.[21] Notably, the emission intensity slightly decreased after the f_w of 80%, which mainly attributes to the serious twisted intramolecular charge transfer (TICT) effect in the polar solvent water.[34] Such effect can be further supported by the emission redshift of 10 nm from 80% to 99% (Figure S8, Supporting Information) and can also be indicated by the typical electron distribution of the highest occupied molecular orbital (HOMO) and lowest unoccupied molecular orbital (LUMO) in both ground and excited states (Figure 1D; and Figure S9, Supporting Information). Additionally, the Stocks shift for TPP-TPA was evaluated to be 220 nm, which is much larger than the small Stokes shifts less than 50 nm in most of commercial NIR fluorophores,[19] avoiding the light contamination of excitation light and self-absorption of emission during biomedical imaging.

The TPP-TPA-loaded NPs were prepared by a nanoprecipitation method as shown in **Figure 2**A. TPP-TPA was formulated using Cor-PEG with bowl-shaped corannulene and DSPE-PEG with linear alkyl chain as the encapsulation matrix, respectively, obtaining Cor-AIE dots and DSPE-AIE dots, which possess similar absorption to TPP-TPA itself in aqueous media (Figure S10, Supporting Information). The sizes of Cor-AIE dots and DSPE-AIE dots were recorded by dynamic light scattering with the values of 46.9 and 49.1 nm, respectively (Figure S11A,B, Supporting Information). Transmission electron microscopy (TEM) was further used to confirm these nanoparticles bearing the spherical shape (Figure S11C,D, Supporting Information). As suggested in Figure 2B, Cor-AIE dots exhibited stronger emission with the quantum yield of 26.8%, which is four times larger than 6.7% for DSPE-AIE dots. Besides, the average fluorescence lifetime of Cor-AIE dots was measured to be 4.34 ns that is about four times as large as that of DSPE-AIE dots (Figure 2C). The fluorescence resonance energy transfer from corannulene to TPP-TPA could be completely ruled out, because the whole absorption spectrum of corannulene and its PEG derivatives are located on the UV range and Cor-PEG exhibits negligible fluorescence under the excitation of 500 nm of Cor-AIE dots (Figure S12A,B, Supporting Information).[35] Therefore, such enhanced emission and lengthened fluorescence lifetime were originated from the enhanced radiative pathway of TPP-TPA.

Furthermore, 9,10-anthracenediyl-bis(methylene)dimalonic acid (ABDA), a commercially available ROS indicator,[36] was used to evaluate the ROS production capacities of Cor-AIE dots and DSPE-AIE dots. Noteworthy, the absorbance of ABDA in water was dramatically decreased in the presence of Cor-AIE dots (Up in Figure 2D) under white light irradiation, whereas faint decrease of ABDA absorbance was observed for DSPE-AIE dots (Down in Figure 2D), suggesting that Cor-AIE dots

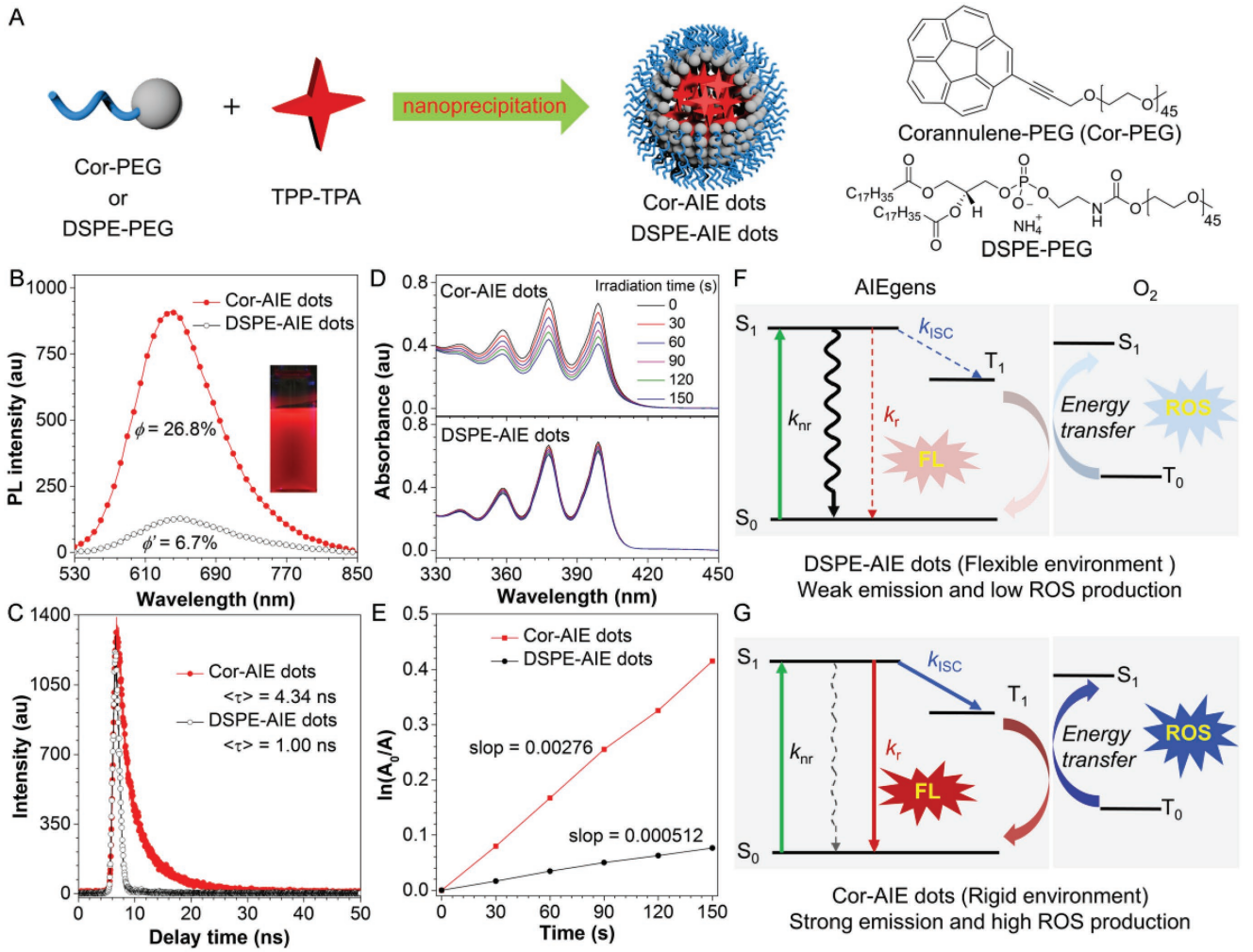

Figure 2. A) Scheme for the preparation of Cor-AIE dots and DSPE-AIE dots using nanoprecipitation method. B) PL and C) fluorescence lifetime spectra of Cor-AIE dots and DSPE-AIE dots. Excitation wavelength: 500 nm. Inset shows the fluorescent photo of Cor-AIE dots taken under 365 nm UV lamp. D) The absorption spectra and E) the decomposition rate of ABDA for Cor-AIE dots (Up) and DSPE-AIE dots (Down) under white light irradiation (60 mW cm^{-2}, 400–1000 nm), where A_0 and A are the absorbance at 378 nm before and after irradiation, respectively. Concentrations of nanoparticles (Cor-AIE dots and DSPE-AIE dots) and ABDA are 0.01 mg mL^{-1} and 100×10^{-6} M, respectively. F,G) Jablonski diagram showing the nonradiative, radiative, and intersystem crossing (ISC) processes for AIEgens in flexible (DSPE-AIE dots) and rigid (Cor-AIE dots) matrixes. S_0: the ground state, S_1: the lowest excited singlet state, T_1: the lowest excited triplet state. k_{nr}, k_r, and k_{ISC} are the rate constants of the nonradiative relaxation, the radiative decay and the ISC process, respectively. FL: fluorescence.

were capable of producing more ROS to decompose ABDA more quickly than DSPE-AIE dots under the same experimental conditions. Plotting of the decomposition rate of ABDA in Figure 2E quantitatively reveals that the ROS generation ability of Cor-AIE dots is around 5.4 times better than that of DSPE-AIE dots, indicative of the far higher ROS production efficiency of Cor-AIE dots.

The underlying principle of such significantly enhanced fluorescence and ROS production was studied. ^{1}H NMR titration experiment was first conducted to investigate the interactions between corannulene and TPP-TPA (**Figure 3**A). Upon stepwise adding corannulene into the CD_2Cl_2 solution of TPP-TPA, the signals of the aromatic protons in 1-methylpyridinium of TPP-TPA gradually shifted upfield by 0.08 ppm (H_a in Figure 3B) and 0.05 ppm (H_b in Figure 3D), while those of the protons in corannulene shifted by about 0.03 ppm (H_e) to the higher field (Figure 3C). Meanwhile, the protons of methyl in 1-methylpyridinium (H_c) and methoxyphenyl (H_d) moieties of TPP-TPA were also shifted by around 0.07 and 0.02 ppm to the upfield, respectively. These chemical shifts evidently imply the unique interactions and the probably relative positions between corannulene and TPP-TPA, with the positively charged 1-methylpyridinium of TPP-TPA closed to the electronegative bottom of corannulene and the TPA and methoxyphenyl units of TPP-TPA outside the bowl of corannulene (Figure 3A; and Figure S13A, Supporting Information), resulting in the shielding effect of corannulene for 1-methylpyridinium of TPP-TPA. Density functional theory (DFT) calculation was also used to study the ISC process (Figure S13B, Supporting Information). The gaps between the S_1 and T_1 states (ΔE_{ST}) for TPP-TPA upon the interaction with corannulene were significantly decreased compared with that for TPP-TPA alone, and the respective spin-orbital coupling (SOC) constants ($\xi(S_1,T_1)$)

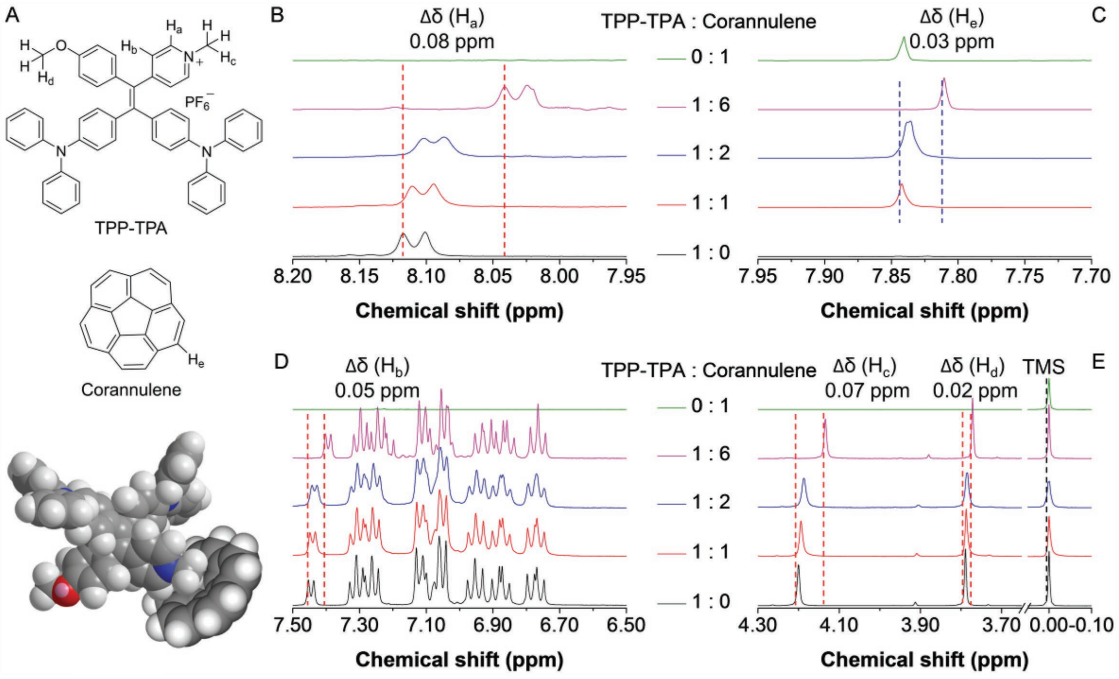

Figure 3. ^{1}H NMR titration experiment with corannulene gradually added into TPP-TPA solution. A) The structures of TPP-TPA and corannulene with featured protons labeled with H_a, H_b, H_c, H_d, and H_e, and the calculated relative position between TPP-TPA and corannulene. B–E) The changes of chemical shifts for TPP-TPA (the aromatic protons of 1-methylpyridinium B,D), the methyl protons in 1-methylpyridinium and anisole E)) and corannulene C) were indicated with the dotted lines (red for TPP-TPA and blue for corannulene) and evaluated by $\Delta\delta$. Concentrations of TPP-TPA was 10×10^{-3} M and corannulene were 10×10^{-3} M (1:1), 20×10^{-3} M (1:2), and 60×10^{-3} M (1:6) in CD_2Cl_2 solution.

between S_1 and T_1 were also increased, suggesting the more accessible ISC process in the presence of corannulene.

Upon getting insight into the molecular structures of corannulene and DSPE, bowl-shaped corannulene possesses a superhydrophobic skeleton and an ultrarigid curvature compared with flexible alkyl-chained DSPE, which hence constructs a more confined microenvironment in aqueous solution. On the other hand, corannulene bears a large dipole moment and the bottom of corannulene bowl is electronegative with the periphery being electropositive, which attract inherent positively charged TPP-TPA by dipole–dipole and electrostatic interactions. As a consequence, when comparing the intraparticle microenvironments of DSPE-AIE dots and Cor-AIE dots, the more confined and rigid microcavity within Cor-AIE dots resulting from the uniqueness of corannulene structure as well as the strong interactions between corannulene and TPP-TPA benefits to restrict the intramolecular rotation of the phenyl rings in TPP-TPA to a much greater extent, which thus inhibits the nonradiative relaxation more effectively. As the absorbed energy of TPP-TPA is fixed, the highly suppressed nonradiative decay for Cor-AIE dots reasonably makes its absorbed energy flow to both the fluorescence pathway and ISC process, achieving significantly amplified emission and ROS generation (Figure 2F,G). This is supported by the theoretical formulas of $\Phi_F = k_r/(k_r + k_{nr} + k_{ISC})$ and $\Phi_{ISC} = k_{ISC}/(k_r + k_{nr} + k_{ISC})$,[37] where the dramatic decrease in nonradiative rate k_{nr} undoubtedly induces the extensive increase of the fluorescence emission efficiency Φ_F and the ISC efficiency Φ_{ISC}. In addition, as TPP-TPA has strong electron donor–acceptor structures in the backbone, the fast process of charge transfer induced fluorescence quenching in aqueous media competes with ROS production.[36] Cor-AIE dots can also provide a more isolated hydrophobic environment to reduce the polar-solvent disruption (such as TICT) for TPP-TPA, bringing about the further enhancement of emission efficiency and ROS production. Indeed, the reduced TICT effect in Cor-AIE dots was reflected by the slight blueshift of about 10 nm in the emission spectrum compared to DSPE-AIE dots (Figure 2B).

Due to the excellent NIR emission output and ROS production, the utility and strength of Cor-AIE dots in cancer phototheranostics were investigated. After we demonstrated that Cor-AIE dots could be internalized in cancer cells and generate ROS within cells effectively (Figure S14, Supporting Information), in vivo studies were carried out using a peritoneal carcinomatosis-bearing mouse model, which was established by intraperitoneal inoculation of murine 4T1 cancer cells. It is worthy to note that the in vivo inoculated 4T1 cancer cells express luciferase, which could emit bioluminescence when the tumor-bearing mice were administrated with the substrate of luciferase (D-luciferin), allowing for precise tracking of the tumor nodules in the mouse peritoneal cavity.[38]

Recently, image-guided cancer surgery using NIR fluorescence has been verified to be feasible during clinical cancer surgery, which holds great promise to promote the outcomes of cancer surgery in the clinic.[39] However, currently available NIR fluorescent probes that are able to meet the necessary requirements of image-guided cancer surgery are still limited. Accordingly, we investigate whether the highly boosted NIR fluorescence in Cor-AIE dots is beneficial to image-guided cancer surgery. In this experiment, the peritoneal carcinomatosis-bearing mouse model was selected, because there are a large number of tumor nodules especially those with diameters <1 mm scattered in the mouse

peritoneal cavity. In the clinic, the submillimeter tumor nodules are difficult to be spotted by surgeon during surgery; however, these remaining small tumors are the major culprits for the in situ cancer recurrence. So far, there have been rather finite NIR fluorescent probes that are capable of accurately examining the submillimeter tumors, mainly because of the low NIR emission output of these probes. This motivates us to assess whether Cor-AIE dots can help surgeon find and remove the ultrasmall tumor nodules with diameters <1 mm.

After the Cor-AIE dots were intravenously injected into the peritoneal carcinomatosis-bearing mice for 24 h, the surgery was performed by opening the mouse abdomen. In vivo NIR fluorescence imaging during surgery indicates that bright Cor-AIE dots fluorescence clearly lights up plenty of tissues as well as their boundaries with rather high signal-to-background ratio (**Figure 4**A; and Figure S15, Supporting Information). As luciferase-expressed 4T1 tumors have bioluminescence, the scattering intraperitoneal tumor nodules are able to be totally and specifically displayed upon bioluminescence imaging postinjection with D-luciferin. As shown in Figure 4A, the bioluminescence signal from luciferase and NIR fluorescence signal from Cor-AIE dots are colocalized perfectly on the surface of the intestines, suggesting that the Cor-AIE dots-visualized tissues are indeed tumors, which are further confirmed by the hematoxylin and eosin (H&E) histological staining. Noteworthy, the fluorescence intensity ratio of tumor to normal intestine is as high as 5.2 for Cor-AIE dots, which exceeds the Rose criterion.[40] Such ratio is significantly higher than those of many reported

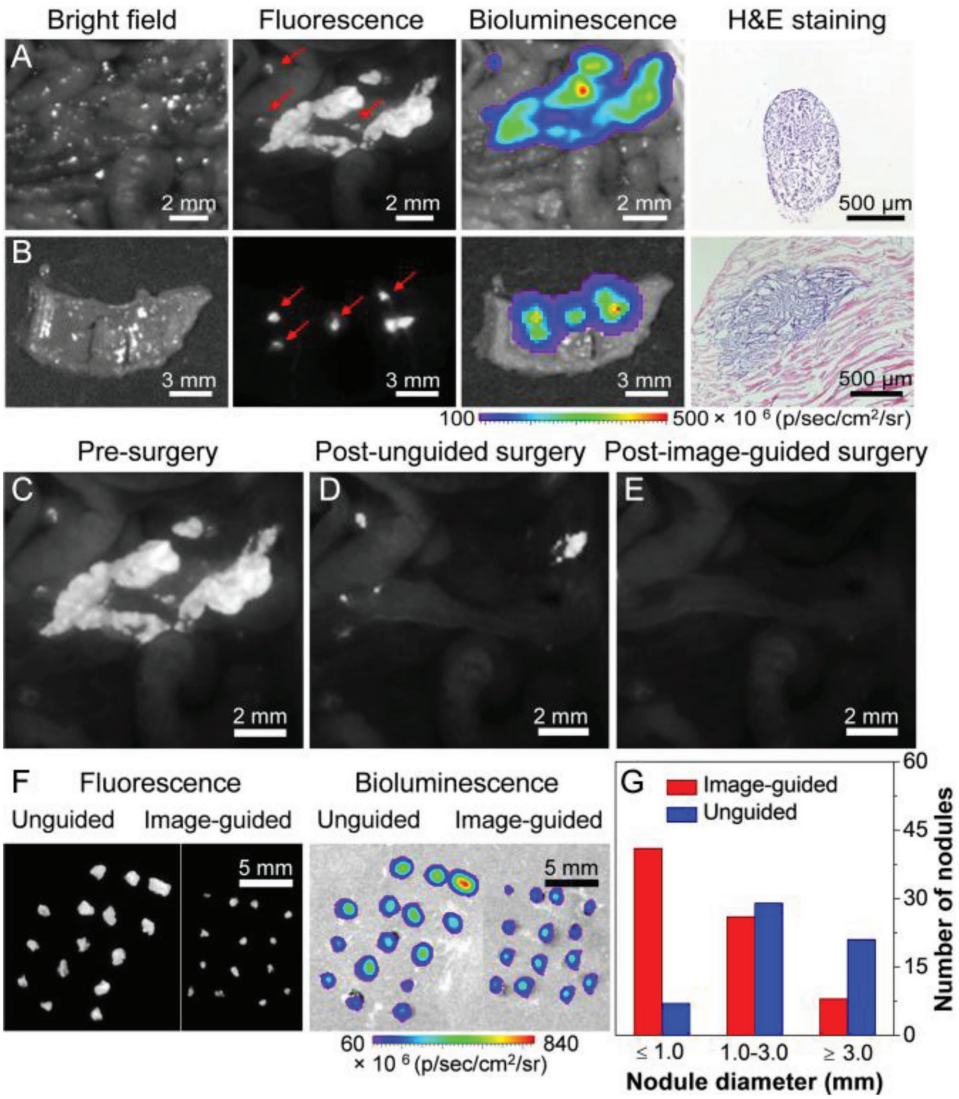

Figure 4. A,B) Bright field, fluorescence, bioluminescence, and H&E staining images of the tumor nodules on the surface of the intraperitoneal intestines A) and the peritoneum B) in peritoneal carcinomatosis-bearing mice after intravenous injection of Cor-AIE dots for 24 h. C–G) Tumor resection with and without Cor-AIE dots fluorescence image-guided surgery. Representative fluorescence images C) before surgery, D) after unguided surgery, and E) after reoperation with the aid of Cor-AIE dots image-guidance. F) The harvested nodules from unguided groups and Cor-AIE dots fluorescence guided groups were examined with a fluorescence imaging system (Left) and a bioluminescence imaging system (Right). G) Histogram of nodule diameters extracted from unguided and Cor-AIE dots fluorescence guided groups.

NIR fluorescent probes including methylene blue and indocyanine green.[41,42] As depicted in Figure 4B, the tumor nodules on the peritoneum are also roughed out with an even larger tumor-to-peritoneum ratio of about 8.0. These results quantitatively demonstrate that the Cor-AIE dots possess remarkable EPR effect, permitting high tumor uptake via passive targeting and thus leading to visualization of intraperitoneal tumor nodules and their boundaries in a specific and high-contrast manner. More importantly, it is also found that the Cor-AIE dots can distinctly delineate the tumor nodules with sizes <1 mm in the peritoneal cavity (indicated by the red arrows in Figure 4), revealing that Cor-AIE dots are efficacious in sharply visualizing submillimeter tumors thanks to their highly boosted NIR emission.

Then the application of the amplified NIR emission of Cor-AIE dots in guidance for surgical tumor removal was studied. To this end, a surgeon from Tianjin First Central Hospital (Tianjin, China) was invited to conduct the operation. As shown in Figure 4C,D, when the surgeon was blinded to the NIR fluorescence imaging by Cor-AIE dots, he removed a lot of intraperitoneal tumors with relatively large diameters (>1 mm) according to his experience. However, after unguided surgery, there are a number of residual tumor nodules remaining in the peritoneal cavity indicated by Cor-AIE dots, which are mainly the ones with diameters <1 mm (Figure 4D). The surgeon then performed a second operation under the guidance of Cor-AIE dots fluorescence, which realizes almost complete removal of the remaining small tumors (Figure 4E–G), confirmed by the negligible intraperitoneal bioluminescence signal. It is noted that all the harvested tumor nodules (mainly submillimeter ones) in the second operation have bioluminescence signals (Figure 4F), validating the precise cancer surgery assisted by Cor-AIE dots. After unguided and Cor-AIE dots fluorescence image-guided surgery, respectively, the survival of the mice was monitored over time with each group containing ten mice. Due to the high malignancy and fast growth of intraperitoneal 4T1 tumors, all the ten mice in unguided surgery group died within 2 weeks. Encouragingly, seven of ten mice in the cohort with Cor-AIE dots fluorescence image-guided surgery are able to survive during 2 week-monitoring duration (Figure S16, Supporting Information). These results together illustrate that Cor-AIE dots greatly promote the cancer surgery outcome by accurately lighting up the submillimeter tumor nodules, considerably prolonging the lifetimes of tumor-bearing mice postoperation.

In many cases in the clinic, the surgeon cannot perform the tumor-removal operation after opening the abdomen, as there are so many small tumors that are hard to be excised completely. As a result, the surgeon has to close the abdominal wall, give up surgery, and choose another treatment strategy. Since in addition to high NIR emission, strong ROS generation ability is the other signature of Cor-AIE dots by virtue of the important contribution of corannulene, we investigated the feasibility of Cor-AIE dots in photodynamic tumor therapy in the aforementioned cases that surgical resection was not suggested after opening the abdomen. To this end, peritoneal carcinomatosis-bearing mice were randomly assigned into five groups, which were designated as "Saline," "Light (L)," "DSPE-AIE dots + L," "Cor-AIE dots + L," and "Cor-AIE dots" with the corresponding treatments described in details in the Experimental Section of the Supporting Information. The tumor size and growth were monitored as the time elapsed through bioluminescence imaging benefitting from the luciferase-expressed 4T1 cancer cells. **Figure 5**A; and Figure S17 (Supporting Information) exhibit the time-dependent bioluminescence imaging of the tumor-bearing mice in each group. It is apparent that tumors with intense bioluminescence signal exist in the abdomen of mice before different treatments on day 0. Dramatically, after receiving the treatment of "Cor-AIE dots + L," the intraperitoneal tumor growth of mice is considerably suppressed, as evidenced by the similar average bioluminescence intensity of intraperitoneal tumors on day 9 to that on day 0 (Figure 5B). As controls, both the treatments of "Cor-AIE dots" and "Light (L)" fail to slow down the growth of intraperitoneal tumors, compared with that of "Saline" (Figure 5B; and Figure S17, Supporting Information), revealing that the highly efficacious anticancer activity in "Cor-AIE dots + L" group roots in the PDT via Cor-AIE dots generating ROS in tumors. It is important to note that the PDT of DSPE-AIE dots does not have any inhibitory effects on tumor growth (Figure 5A,B). This result not only indicates the high malignancy of intraperitoneal tumors, but also implies that the ROS production ability of DSPE-AIE dots is not strong enough to work in this tumor-bearing animal model. The treatment of "Cor-AIE dots + L" leads to greatly prolonged lifetimes of mice and the median survival time for "Cor-AIE dots + L" group is far longer than that for "DSPE-AIE dots + L" group (Figure 5C). The sharp comparison in the antitumor efficacy between the PDT of Cor-AIE dots and DSPE-AIE dots reasonably highlights the necessity and importance of our new approach to superior AIE dots.

In summary, we have first reported that enhancing the intraparticle confined microenvironment could serve as an effective approach to guiding the design of superior AIE dots with both highly amplified fluorescence and ROS production, benefitting to greatly improved cancer phototheranostics in vivo. With facile introduction of two electron-donating diphenylamine groups and one electron-withdrawing 1-methylpyridinium unit into the triphenylethene, a new NIR emissive AIEgens, namely TPP-TPA, was simply synthesized, featured with "rotor-rich" skeleton and an inherent charge. Then, encapsulation of TPP-TPA with DSPE-PEG or Cor-PEG afforded DSPE-AIE dots or Cor-AIE dots with different intraparticle rigid microenvironments. Compared to DSPE-AIE dots, Cor-AIE dots exhibited 4.0-fold amplified fluorescence quantum yield and 5.4-fold enhanced ROS production. As corannulene possesses large dipole moment of 2.1 D, superhydrophobicity, hyper rigidity, and uneven electron distribution, it provides larger intraparticle rigidity. Together with the strong interactions between corannulene and TPP-TPA indicated by ^{1}H NMR titration, the intraparticle confined microenvironment in Cor-AIE dots forcefully restricts the intramolecular rotation of the encapsulated TPP-TPA and highly suppresses its nonradiative decay leading to the flow of excited-state energy to both the fluorescence pathway and ISC process, which were also supported by theoretical calculation. Such high NIR emission and ROS production tremendously promoted the phototheranostic efficacies in terms of NIR image-guided cancer surgery and PDT with a peritoneal carcinomatosis-bearing mouse model. This study not only brings in a new category of corannulene-based

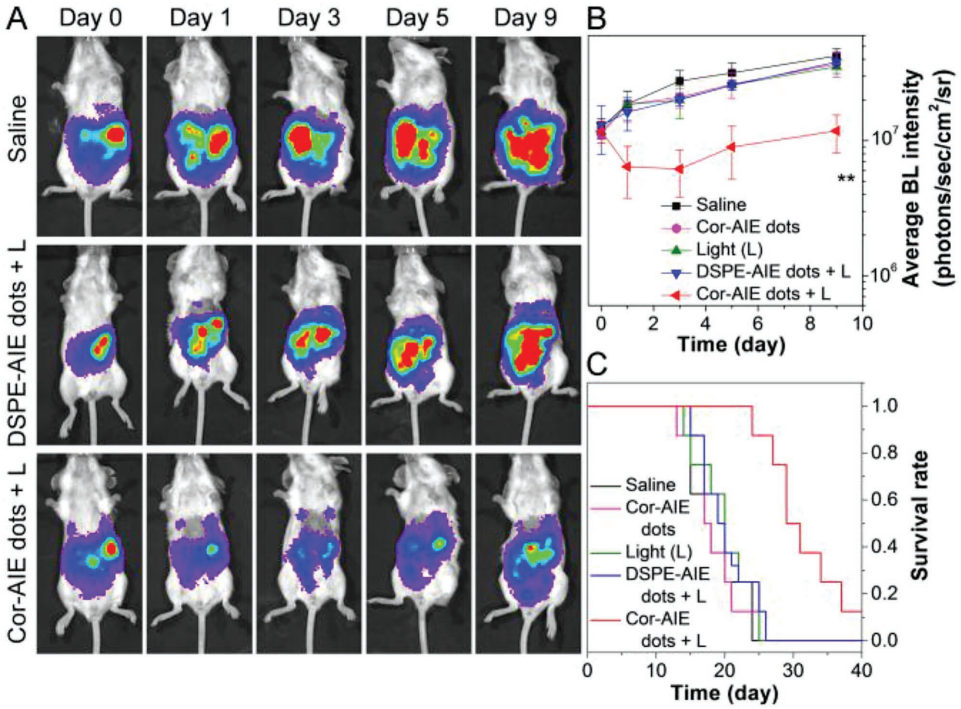

Figure 5. A) The time-dependent bioluminescence imaging of the peritoneal carcinomatosis-bearing mice in "Saline," "DSPE-AIE dots + L," and "Cor-AIE dots + L" groups. B) The average bioluminescence (BL) intensities of intraperitoneal tumors on days 0, 1, 3, 5, and 9 in various groups indicated. **represents $P < 0.01$, in comparison between the average BL intensity of intraperitoneal tumors in "Cor-AIE dots + L" cohort and other groups. C) The curve of survival rate after different treatments. All the experiment groups are "Saline," "Cor-AIE dots," "Light (L)," "DSPE-AIE dots + L," and "Cor-AIE dots + L." "L" is under the white light (0.4 W cm^{-2}) for 10 min. The concentrations of DSPE-AIE dots and Cor-AIE dots injected are 1 mg mL^{-1} based on TPP-TPA. The volume of injection is 150 µL.

AIE dots with superior biomedical performances, but also reasonably demonstrates that enhancing the intraparticle confined microenvironment that further inhibits the nonradiative decay of encapsulated AIEgens is a unique and new strategy to prepare AIE dots with both highly enhanced fluorescence and ROS generation capacity. This underlying principle to highly boost the phototheranostic efficacy should also be beneficial to other fluorescent NPs systems.

Supporting Information

Supporting Information is available from the Wiley Online Library or from the author.

Acknowledgements

X.G. and X.Z. contributed equally to this work. This work was partially supported by the National Natural Science Foundation of China Grant (Nos. 21502022, 21788102, 51622305, and 21702016), the National Basic Research Program of China (Nos. 973 Program, 2015CB856503, 2013CB834701, and 2013CB834702), the Innovation and Technology Commission (No. ITC-CNERC14SC01), the Research Grants Council of Hong Kong (Nos. 16308016, 16305015, C2014-15G, N_HKUST604/14, and A-HKUST605/16), and the Science and Technology Plan of Shenzhen (No. JCYJ20160229205601482). D.D. thanks the PCSIRT (No. IRT13023), the Science & Technology Project of Tianjin of China (No. 15JCYBJC29800), and the 111 project (No. B08011). All animal studies were performed in compliance with the guidelines set by Tianjin Committee of Use and Care of Laboratory Animals and the overall project protocols were approved by the Animal Ethics Committee of Nankai University.

Conflict of Interest

The authors declare no conflict of interest.

Keywords

aggregation-induced emission, AIE nanodots, cancer phototheranostics, near-infrared fluorescence image-guided surgery, photodynamic therapy

Received: February 13, 2018
Revised: March 19, 2018
Published online:

[1] S. Kunjachan, J. Ehling, G. Storm, F. Kiessling, T. Lammers, *Chem. Rev.* **2015**, *115*, 10907.
[2] C. Chu, H. Lin, H. Liu, X. Wang, J. Wang, P. Zhang, H. Gao, C. Huang, Y. Zeng, Y. Tan, G. Liu, X. Chen, *Adv. Mater.* **2017**, *29*, 1605928.
[3] H. Fan, G. Yan, Z. Zhao, X. Hu, W. Zhang, H. Liu, X. Fu, T. Fu, X. B. Zhang, W. Tan, *Angew. Chem., Int. Ed.* **2016**, *55*, 5477.
[4] G. Tian, X. Zhang, Z. Gu, Y. Zhao, *Adv. Mater.* **2015**, *27*, 7692.

[5] X. Chen, S. S. Gambhir, J. Cheon, *Acc. Chem. Res.* **2011**, *44*, 841.
[6] K. K. Ng, G. Zheng, *Chem. Rev.* **2015**, *115*, 11012.
[7] X. Ai, J. Mu, B. Xing, *Theranostics* **2016**, *6*, 2439.
[8] C. Wang, L. Xu, C. Liang, J. Xiang, R. Peng, Z. Liu, *Adv. Mater.* **2014**, *26*, 8154.
[9] M. P. Melancon, M. Zhou, C. Li, *Acc. Chem. Res.* **2011**, *44*, 947.
[10] Y. Li, T. Lin, Y. Luo, Q. Liu, W. Xiao, W. Guo, D. Lac, H. Zhang, C. Feng, S. Wachsmann-Hogiu, J. H. Walton, S. R. Cherry, D. J. Rowland, D. Kukis, C. Pan, K. S. Lam, *Nat. Commun.* **2014**, *5*, 4712.
[11] H. Wang, P. Agarwal, S. Zhao, J. Yu, X. Lu, X. He, *Nat. Commun.* **2014**, *6*, 10081.
[12] Q. Fan, K. Cheng, Z. Yang, R. Zhang, M. Yang, X. Hu, X. Ma, L. Bu, X. Lu, X. Xiong, W. Huang, H. Zhao, Z. Cheng, *Adv. Mater.* **2015**, *27*, 843.
[13] T. L. Doanea, C. Burda, *Chem. Soc. Rev.* **2012**, *41*, 2885.
[14] J. A. Barreto, W. O'Malley, M. Kubeil, B. Graham, H. Stephan, L. Spiccia, *Adv. Mater.* **2011**, *23*, H18.
[15] Y. Liu, T. Chen, C. Wu, L. Qiu, R. Hu, J. Li, S. Cansiz, L. Zhang, C. Cui, G. Zhu, M. You, T. Zhang, W. Tan, *J. Am. Chem. Soc.* **2014**, *136*, 12552.
[16] G. Chen, I. Roy, C. Yang, P. N. Prasad, *Chem. Rev.* **2016**, *116*, 2826.
[17] a) A. Reisch, A. S. Klymchenko, *Small* **2016**, *12*, 1968; b) K. Trofymchuk, A. Reisch, P. Didier, F. Fras, P. Gilliot, Y. Mely, A. S. Klymchenko, *Nat. Photonics* **2017**, *11*, 657.
[18] A. Master, M. Livingston, A. Sen Gupta, *J. Controlled Release* **2013**, *168*, 88.
[19] X. Gu, R. T. K. Kwok, J. W. Y. Lam, B. Z. Tang, *Biomaterials* **2017**, *146*, 115.
[20] D. Ding, K. Li, B. Liu, B. Z. Tang, *Acc. Chem. Res.* **2013**, *46*, 2441.
[21] a) J. Mei, N. L. C. Leung, R. T. K. Kwok, J. W. Y. Lam, B. Z. Tang, *Chem. Rev.* **2015**, *115*, 11718; b) J. Mei, Y. Hong, J. W. Y. Lam, A. Qin, Y. Tang, B. Z. Tang, *Adv. Mater.* **2014**, *26*, 5429.
[22] X. Wu, X. Sun, Z. Guo, J. Tang, Y. Shen, T. D. James, H. Tian, W. H. Zhu, *J. Am. Chem. Soc.* **2014**, *136*, 3579.
[23] A. Shao, Y. Xie, S. Zhu, Z. Guo, S. Zhu, J. Guo, P. Shi, T. D. James, H. Tian, W. H. Zhu, *Angew. Chem., Int. Ed.* **2015**, *54*, 7275.
[24] K. Gu, Y. Xu, H. Li, Z. Guo, S. Zhu, P. Shi, T. D. James, H. Tian, W. H. Zhu, *J. Am. Chem. Soc.* **2016**, *138*, 5334.
[25] M. Li, Y. Gao, Y. Yuan, Y. Wu, Z. Song, B. Z. Tang, B. Liu, Q. C. Zheng, *ACS Nano* **2017**, *11*, 3922.
[26] X. Wang, J. Hu, G. Zhang, S. Liu, *J. Am. Chem. Soc.* **2014**, *136*, 9890.
[27] a) W. Wu, D. Mao, F. Hu, S. Xu, C. Chen, C. J. Zhang, X. Cheng, Y. Yuan, D. Ding, D. Kong, B. Liu, *Adv. Mater.* **2017**, *29*, 1700548; b) X. Zhen, Y. Tao, Z. An, P. Chen, C. Xu, R. Chen, W. Huang, K. Pu, *Adv. Mater.* http://doi.org/10.1002/adma.201606665.
[28] F. Hu, Y. Huang, G. Zhang, R. Zhao, H. Yang, D. Zhang, *Anal. Chem.* **2014**, *86*, 7987.
[29] G. Feng, B. Liu, *Small* **2016**, *12*, 6528.
[30] K. Shi, T. Lei, X. Y. Wang, J. Y. Wang, J. Pei, *Chem. Sci.* **2014**, *5*, 1041.
[31] B. M. Schmidt, T. Osuga, T. Sawada, M. Hoshino, M. Fujita, *Angew. Chem., Int. Ed.* **2016**, *55*, 1561.
[32] M. Juríček, N. L. Strutt, J. C. Barnes, A. M. Butterfield, E. J. Dale, J. J. Baldridge, J. Fraser Stoddart, J. S. Siegel, *Nat. Chem.* **2014**, *6*, 222.
[33] a) X. Gu, E. Zhao, J. W. Y. Lam, Q. Peng, Y. Xie, Y. Zhang, K. S. Wong, H. H. Y. Sung, I. D. Williams, B. Z. Tang, *Adv. Mater.* **2015**, *27*, 7093; b) X. Gu, E. Zhao, T. Zhao, M. Kang, C. Gui, J. W. Y. Lam, S. Du, M. M. T. Loy, B. Z. Tang, *Adv. Mater.* **2016**, *28*, 5064.
[34] Z. R. Grabowski, K. Rotkiewicz, *Chem. Rev.* **2003**, *103*, 3899.
[35] P. Bachawala, T. Ratterman, N. Kaval, J. Mack, *Tetrahedron* **2017**, *73*, 3831.
[36] W. Wu, G. Feng, S. Xu, B. Liu, *Macromolecules* **2016**, *49*, 5017.
[37] Q. Peng, Y. Niu, Q. Wu, X. Gao, Z. Shuai, *Aggregation-Induced Emission: Fundamentals and Applications*, Vols. 1 and 2, John Wiley and Sons Ltd, Hoboken, NJ, USA **2013**, Ch. 17.
[38] J. Liu, C. Chen, S. Ji, Q. Liu, D. Ding, D. Zhao, B. Liu, *Chem. Sci.* **2017**, *8*, 2782.
[39] A. L. Vahrmeijer, M. Hutteman, J. R. van der Vorst, C. J. H. van de Velde, J. V. Frangioni, *Nat. Rev. Clin. Oncol.* **2013**, *10*, 507.
[40] A. L. Antaris, H. Chen, K. Cheng, Y. Sun, G. Hong, C. Qu, S. Diao, Z. Deng, X. Hu, B. Zhang, X. Zhang, O. K. Yaghi, Z. R. Alamparambil, X. Hong, Z. Cheng, H. Dai, *Nat. Mater.* **2016**, *15*, 235.
[41] C. T. Zeng, W. T. Shang, K. Wang, C. W. Chi, X. H. Jia, C. Fang, D. Yang, J. Z. Ye, C. H. Fang, J. Tian, *Sci. Rep.* **2016**, *6*, 21959.
[42] O. T. Okusanya, D. Holt, D. Heitjan, C. Deshpande, O. Venegas, J. Jiang, R. Judy, E. DeJesus, B. Madajewski, K. Oh, M. Wang, S. M. Albelda, S. Nie, S. Singhal, *Ann. Thorac. Surg.* **2014**, *98*, 1223.